Dynamics and Self-Propulsion of a Spherical Body Shedding Coaxial Vortex Rings in an Ideal Fluid

Phanindra Tallapragada Scott David Kelly
Department of Mechanical Engineering and Engineering Science
University of North Carolina at Charlotte

We describe a model for the dynamic interaction of a sphere with uniform density and a system of coaxial circular vortex rings in an ideal fluid of equal density. At regular intervals in time, a constraint is imposed that requires the velocity of the fluid relative to the sphere to have no component transverse to a particular circular contour on the sphere. In order to enforce this constraint, new vortex rings are introduced in a manner that conserves the total momentum in the system. This models the shedding of rings from a sharp physical ridge on the sphere coincident with the circular contour. If the position of the contour is fixed on the sphere, vortex shedding is a source of drag. If the position of the contour varies periodically, propulsive rings may be shed in a manner that mimics the locomotion of certain jellyfish. We present simulations representing both cases.

I. INTRODUCTION

When a solid body moves through a viscous fluid, a boundary layer forms on the body. The fluid velocity varies across this layer to reconcile the no-slip condition on the body's surface with the behavior of the fluid far away. Under certain circumstances, a body's geometry and motion may conspire to cause the boundary layer to detach at a particular location. When a wing is drawn through the air, for instance, the boundary layers formed atop and below the wing detach, by design, at the wing's trailing edge. The abrupt relaxation of the no-slip condition at one extreme of a detaching boundary layer causes the fluid within to roll over as it separates from the body. The body experiences a force due to boundary layer detachment; the fluid attains vorticity in the balance.

Vortex shedding plays an essential role in diverse mechanisms for aquatic propulsion. The fins of many fish and marine mammals, for instance, represent analogues of the wing described above. When vorticity is shed from the trailing edge of an undulating fin, the local transfer of momentum to the water is balanced by the development of thrust on the fin. In the present paper, we describe a model for the locomotion of certain jellyfish, called medusae, that possess bell-like bodies. As a medusan bell opens and closes, vortex rings are shed from the lip of the bell, imparting backward momentum to the fluid and forward momentum to the animal. This is studied empirically in [1] and depicted schematically in Fig. 1. The swimming body in our model is assumed to remain spherical, but a circular curve on the body is assigned special significance as a surrogate for the moving lip, and grows and shrinks over time to mediate the propulsive shedding of vortex rings.

The idealized representation of circumstances leading to localized vortex shedding in terms of fluid velocity constraints originated with the *Kutta-Zhukovskii condition* concerning separation at the trailing edge of an airfoil [2]. The introduction of this condition to an inviscid model for the flow over a planar foil is sufficient to engender the accurate prediction of lift on the foil without explicit reference to viscosity. Variations of this idea have been employed in studying the wakes of delta wings [3], oscillating cylinders [4], and planar fishlike swimmers [5–8] and recently the dynamic interactions of falling cards, flapping flags, and self-propelled hydrofoils with unsteady shed point vortices [9–11]. Interestingly, the idea of introducing vortex filaments with curvature, such as circular vortex rings, to study propulsion in three dimensions has not been explored so far. The present work is a first step along these lines.

The model we present is based on the inviscid hydrodynamics of a spherical body interacting with singular vortex filaments, and we also eschew the explicit attribution of vortex shedding to viscosity. Instead, we suppose the special moving curve on the body's surface to be an idealized barrier to transverse flow. Just as a viscous fluid will detach rather than flow around a sharp ridge on a real surface, the inviscid fluid in our model is prohibited from crossing the specified curve. Vortex rings are introduced to the flow adjacent to this curve to correct the transverse flow speed at regular intervals in time. With the shedding of each ring modeled in this way, the momentum of the fluid changes discontinuously, but the momentum of the body is amended simultaneously to maintain the conservation of momentum overall.

The simplified depiction of Fig. 1 suggests that a single vortex ring is shed each time a jellyfish closes its bell. In reality, vorticity is shed continuously, and the overall concentration of this vorticity into coherent propulsive rings with significant strength is a result of variations over time in the strength of the vorticity being shed and of subsequent hydrodynamic interactions. In our model, vorticity isn't shed continuously, but rings of differential strength are shed at a frequency much greater than that at which the shedding contour oscillates. These rings represent a discrete approximation to an axisymmetric vortex sheet that forms coherent propulsive structures dynamically. In a future paper, the model presented herein will be compared directly to one in which the restriction of transverse flow across

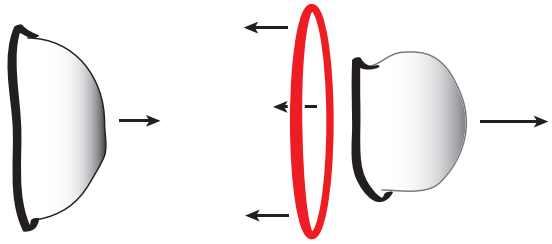

FIG. 1: A single swimming stroke by a medusan jellyfish. As the bell closes, a vortex ring is shed from its lip, inducing net motion of the fluid behind the jellyfish to the left and propelling the jellyfish to the right.

the shedding contour is enforced continuously through the development of rings with time-varying strength. The rings in the present paper may differ in strength from one another, but the strength of each is constant once it's been shed.

Noncanonical Hamiltonian structures have recently been shown to underlie the interactions of free bodies with singular distributions of vorticity in both two-dimensional [12–15] and three-dimensional [16] ideal fluids. Between vortex shedding events, the body and vortex rings in the model presented herein interact according to the Hamiltonian equations presented in [16], specialized as in [17] to the case in which the body is spherical, the rings are circular, and the body and rings are coaxial. The simultaneous introduction of a control parameter and a mechanism for vortex shedding to the model from [17] parallels the progression from [15] to [8], through which a Hamiltonian model for the interaction of a free planar body with a system of point vortices was developed into a model for fishlike locomotion.

II. MODELING

In presenting the model introduced above, we make use of the following symbols:

M, a	effective mass and radius of the sphere, respectively
$\mathbf{L}$, $\mathbf{P}$	total linear impulse in the system and linear impulse of the fluid due to vorticity, respectively
H	Hamiltonian
$\mathbf{U}$	velocity of the sphere
$\mathbf{n}$	outward unit normal vector on the sphere
$\mathbf{u}$	velocity field of the fluid
$\mathbf{u}_V$	velocity field due to vorticity
$\mathbf{u}_{Rj}$	velocity field due to the jth vortex ring
$\mathbf{u}_{Ij}$	velocity field due to the image in the sphere of the jth vortex ring
$\mathbf{u}_{Sj}$	self-induced velocity of the jth ring
$\mathbf{\Phi}_B$	Kirchhoff potential
Γ_j, z_j, R_j	circulation, translational position, and radius of the jth vortex ring, respectively
θ	azimuthal angle of the circle on the sphere along which vortex shedding occurs
d	parameter specifying the initial radius R_j of the jth vortex ring such that $R_j = (a+d)\sin\theta$.
$\mathbf{l}$	vector position of a point in coordinates attached to the center of the sphere
$\mathbf{l}_j$, $\bar{\mathbf{l}}_j$	vector position of a point on the jth vortex ring and its image inside the sphere, respectively
$\hat{\mathbf{x}}$, $\hat{\mathbf{y}}$, $\hat{\mathbf{z}}$	unit vectors in the spatial x, y, and z directions, respectively
$\mathbf{e}_\mathbf{l}$, $\mathbf{e}_{\mathbf{l}j}$	unit vectors along $\mathbf{l}$ and $\mathbf{l}_j$, respectively
$\mathbf{t}_j$	unit vector vector tangent to the jth vortex ring
C_j	arclength-parameterized curve representing the jth vortex ring
s_j	arclength parameter along the jth vortex ring

A. Hamiltonian structure

It was demonstrated in [16] that under certain relatively permissive technical assumptions, the equations governing the interaction of a free solid body with a system of closed vortex filaments in a three-dimensional ideal fluid possess a Hamiltonian structure. For the simple case in which the body is a sphere and the filaments are coaxial vortex rings situated along an axis intersecting the sphere's center, the dynamics of this system were studied computationally in [17]. We take the model in [17], which we review here, as our starting point.

The model consists of a free solid sphere with radius a in an ideal fluid that extends to infinity in all directions. The sphere and fluid are assumed to have uniform unit density. The compact subset of $\mathbb{R}^3$ occupied by the sphere is denoted by $\mathcal{B}$ and its boundary by $\partial\mathcal{B}$. The unbounded fluid domain external to the sphere is denoted by $\mathcal{D} = \mathbb{R}^3 \setminus \mathcal{B}$. As the sphere moves in the fluid, the normal velocity of the fluid relative to the sphere is zero on $\partial\mathcal{B}$. Vorticity in the fluid is assumed to be confined to a delta distribution on N vortex rings, corresponding to closed curves in $\mathbb{R}^3$, that intersect neither the sphere nor one another. Later we will relax this assumption by giving the vortex rings a core of a small volume to account for their self-induced velocity. The Helmholtz decomposition allows the fluid velocity field to be written as

$$\mathbf{u} = \nabla\mathbf{\Phi}_B + \mathbf{u}_V, \tag{1}$$

where the first component on right-hand side of the equation is the velocity due to the motion of the sphere and the second component is the velocity due to the vortex rings. The individual components of $\mathbf{u}$ must satisfy

$$\nabla^2\mathbf{\Phi}_B = 0$$
$$\nabla \cdot \mathbf{u}_V = 0$$

in the fluid domain $\mathcal{D}$, with the boundary conditions

$$\nabla\mathbf{\Phi}_B|_{\partial\mathcal{B}} \cdot \mathbf{n} = \mathbf{U} \cdot \mathbf{n}$$
$$\mathbf{u}_V|_{\partial\mathcal{B}} \cdot \mathbf{n} = 0,$$

where $\mathbf{U}$ is the velocity of the sphere.

The gradient of the Kirchhoff potential is assumed to decrease with distance from the sphere sufficiently quickly that $\int_{\mathcal{D}}\langle\nabla\mathbf{\Phi}_B, \nabla\mathbf{\Phi}_B\rangle dV$ is bounded. In this case, the total kinetic energy of the fluid and the sphere can be written in the form

$$T = \frac{1}{2}\int_{\mathcal{D}}\langle\mathbf{u}_V, \mathbf{u}_V\rangle dV + \frac{1}{2}\langle\mathbf{U}, M\mathbf{U}\rangle,$$

where M is the *effective mass* of the sphere, i.e., the mass of the sphere plus the added mass due to its motion [18]. Unlike planar point vortices, curved vortex filaments in three dimensions exhibit self-induced motion. The self-induced velocity of the filaments in our model must be regularized, as discussed in [18, 19], in order for the total kinetic energy T to be bounded. Once this is done, the system possesses a Hamiltonian structure with the kinetic energy as the Hamiltonian.

The Lie-Poisson equations governing the motion of the sphere and rings together, derived in [16, 17], take the form

$$\frac{d}{dt}(M\mathbf{U} + \mathbf{P}) = 0. \tag{2}$$

The total linear impulse $\mathbf{L} = M\mathbf{U} + \mathbf{P}$ includes both a component due to the motion of the sphere and a component, to be discussed in detail below, due to the vortex rings. It's clear from (2) that if a mechanism is introduced whereby impulse can be imparted to the fluid through vortex shedding, that mechanism can form the basis for propelling the sphere.

B. Calculation of the velocity field and the linear impulse

Associated with a vortex ring outside a sphere is an image ring inside the sphere [18, 20], as depicted in Fig. 2. In combination, the external ring and its image induce a velocity field that satisfies the impenetrability condition on the sphere's surface. The position of the image ring is determined by the Kelvin transformation. The solenoidal velocity $\mathbf{u}_V$ in (1) is the sum of the velocities due to the N external rings, denoted individually by $\mathbf{u}_{Rj}$, and the velocities due to their image rings, denoted individually by $\mathbf{u}_{Ij}$.

If q is a point with vector position $\mathbf{l} = (x, y, z)$ relative to a frame of reference fixed at the center of the sphere as shown in in Fig. 2, then the fluid velocity at q due to the jth vortex ring is given by the Biot-Savart law as

$$\mathbf{u}_{Rj}(q) = \frac{\Gamma_j}{4\pi}\oint_{C_j}\frac{\mathbf{t}_j \times (\mathbf{l} - \mathbf{l}_j)}{|\mathbf{l} - \mathbf{l}_j|^3} ds_j, \tag{3}$$

where $\mathbf{l}_j$ denotes the position vector of a point on the jth ring and $\mathbf{t}_j$ the unit vector tangent to the jth ring at this point. Following [17, 21], the mth component of the fluid velocity at the point q due to the ith image ring is given by

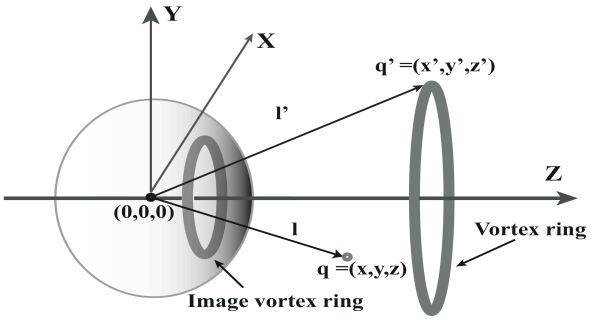

FIG. 2: A free sphere, a coaxial circular vortex ring, and the image of the ring in the sphere. Interaction of the sphere and the ring will cause both to translate along the z axis and the radius of the ring to vary.

$$(\mathbf{u}_{Ii})^m = \frac{-\Gamma_i}{4\pi a}\oint_{C_i}\left\langle \mathfrak{Q}_i(\mathbf{l},\mathbf{l_i})\frac{\partial \mathbf{e_l}}{\partial \mathbf{e}_m} + \left(\mathfrak{X}_i(\mathbf{l},\mathbf{l_i})a^2 x_m + \mathfrak{A}_i(\mathbf{l},\mathbf{l_i})\left\langle \mathbf{e}_{\mathbf{l}i}, \frac{\partial \mathbf{e_l}}{\partial \mathbf{e}_m}\right\rangle\right), \mathbf{e}_{\mathbf{l}i}\times \mathbf{t}_i\right\rangle ds_i,$$

where $(x_1,x_2,x_3)=(x,y,z)$, $(\mathbf{e}_1,\mathbf{e}_2,\mathbf{e}_3)=(\hat{\mathbf{x}},\hat{\mathbf{y}},\hat{\mathbf{z}})$, $\mathbf{e_l}=\frac{\mathbf{l}}{|\mathbf{l}|}$, $\mathbf{e}_{\mathbf{l}i}=\frac{\mathbf{l}_i}{|\mathbf{l}_i|}$, and

$$\begin{aligned}
\mathfrak{Q}_i(\mathbf{l},\mathbf{l_i}) &= \frac{|\bar{\mathbf{l}}|^2}{|\mathbf{l}_i||\bar{\mathbf{l}}-\mathbf{l}_i|\left(\frac{|\bar{\mathbf{l}}-\mathbf{l}_i|}{|\mathbf{l}_i|}+1-\frac{1}{|\mathbf{l}_i|^2}\langle\bar{\mathbf{l}},\mathbf{l}_i\rangle\right)},\\
\mathfrak{X}_i(\mathbf{l},\mathbf{l_i}) &= \frac{|\mathbf{l}_i||\bar{\mathbf{l}}|}{|\mathbf{l}_i|^3|\bar{\mathbf{l}}-\bar{\mathbf{l}}_i|^3},\\
\mathfrak{A}_i(\mathbf{l},\mathbf{l_i}) &= \frac{|\bar{\mathbf{l}}|^3}{|\mathbf{l}_i|^2|\bar{\mathbf{l}}-\mathbf{l}_i|}\frac{\frac{|\bar{\mathbf{l}}-\mathbf{l}_i|^2}{|\bar{\mathbf{l}}|^2}+2\frac{|\bar{\mathbf{l}}-\mathbf{l}_i|}{|\bar{\mathbf{l}}|}+1-\frac{1}{|\mathbf{l}_i|^2}\langle\bar{\mathbf{l}},\mathbf{l}_i\rangle}{\left(\frac{|\bar{\mathbf{l}}-\mathbf{l}_i|^2}{|\bar{\mathbf{l}}|^2}+\frac{|\bar{\mathbf{l}}-\mathbf{l}_i|}{|\bar{\mathbf{l}}|}\left(1-\frac{1}{|\mathbf{l}_i|^2}\langle\bar{\mathbf{l}},\mathbf{l}_i\rangle\right)\right)}.
\end{aligned}$$

The overbar in the last three expressions denotes the image in the sphere of the vector it modifies.

A vortex filament with nonzero curvature has a self-induced velocity. This is apparent from the Biot-Savart law, but invoking (3) to compute the velocity of a point on the jth ring due to the influence of that ring leads to a logarithmic divergence. A classical approach to overcome this divergence is the *local induction approximation*, which requires the core of a vortex ring to have a small volume [18, 19, 22, 23]. The volume of the core is such that the radius of the core is small compared to the radius of the ring. According to the local induction approximation, the self-induced velocity of the ith vortex ring is given by

$$\mathbf{u}_{Si} = \frac{\Gamma_i}{4\pi R_i}\left(\log\frac{8R_i}{c_i}-\frac{1}{4}\right)\hat{\mathbf{z}},$$

where $c_i^2 R_i$ is taken to be the volume of the ring.

The Kirchhoff potential $\mathbf{\Phi}_B$ is given, according to [18, 24], by

$$\mathbf{\Phi}_B = -\frac{a^3 x}{2|\mathbf{l}|^3}U_x - \frac{a^3 y}{2|\mathbf{l}|^3}U_y - \frac{a^3 z}{2|\mathbf{l}|^3}U_z, \tag{4}$$

where $\mathbf{U}=(U_x,U_y,U_z)$. The contribution $\mathbf{P}$ of the vortex rings to the total linear impulse is given by

$$\mathbf{P} = \sum_{i=1}^{N}\left(\Gamma_i\pi R_i^2 - \frac{a}{2}I_i(z_i,R_i;a,\Gamma_i)\right), \tag{5}$$

where $I_i(z_i,R_i;a,\Gamma_i)$ is defined so that

$$I_i(z_i,R_i;a,\Gamma_i)\hat{\mathbf{z}} = \int_{\partial\mathcal{B}}(\mathbf{u}_{Ri}+\mathbf{u}_{Vi})dA.$$

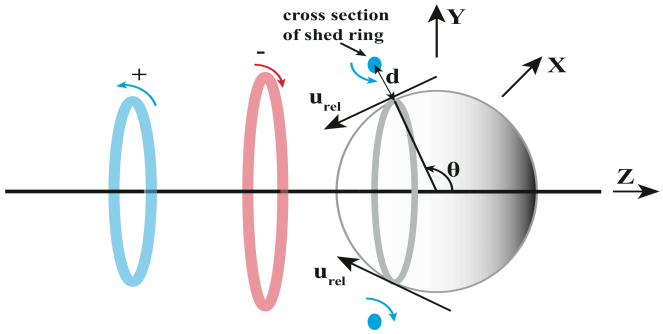

FIG. 3: A new vortex ring is introduced to the fluid at a distance $a+d$ from the center of the sphere, directly above a circular contour on the sphere representing a ridge like the lip of the bell in Fig. 1. The strength of the ring is selected to nullify the relative fluid velocity tangent to the sphere and transverse to the contour; the momentum of the sphere is adjusted simultaneously to preserve the total linear impulse in the system. Vortex rings shed at earlier instants in time evolve nearby; these are shaded according to their circulations.

The equality in (5) is obtained, following [13, 16], by applying the Reynolds transport theorem to the fluid momentum in $\mathcal{D}$. With these substitutions, the positions of the sphere and rings along the z axis and the radii of the rings evolve such that

$$\begin{aligned}
\mathbf{U} &= \frac{1}{M}(\mathbf{L}-\mathbf{P}),\\
\dot{z}_i &= -\mathbf{U} + \left(\mathbf{u}_{Si} + \sum_{j=1\,(j\neq i)}^{N} \mathbf{u}_{Rj}(\mathbf{l}_i) + \sum_{j=1}^{N} \mathbf{u}_{Ij}(\mathbf{l}_i) + \nabla\mathbf{\Phi}_B\right)\cdot\hat{\mathbf{z}},\\
\dot{R}_i &= \left(\sum_{j=1\,(j\neq i)}^{N} \mathbf{u}_{Rj}(\mathbf{l}_i) + \sum_{j=1}^{N} \mathbf{u}_{Ij}(\mathbf{l}_i) + \nabla\mathbf{\Phi}_B\right)\cdot\hat{\mathbf{y}},
\end{aligned} \tag{6}$$

where $i = 1, 2, \ldots, N$.

C. Creation of new vortex rings

Newly shed vortex rings are introduced to our model in a manner analogous to that employed in [8] to introduce shed point vortices near the trailing cusp of a free planar hydrofoil. In that paper, a Kutta-Zhukovskii condition is enforced at regular intervals in time at this cusp in tandem with the conservation of linear and angular impulse. With the shedding of each point vortex, the foil experiences an impulsive change in momentum. In the present context, we augment the model described in the preceding paragraphs with a mechanism whereby circular vortex rings are shed at regular intervals in time into the fluid adjacent to a particular circular contour on the sphere, as shown in Fig. 3. This contour represents a sharp ridge across which fluid in contact with the the sphere cannot flow; the position and strength of each shed ring are selected to nullify the flow tangent to the sphere and transverse to the ridge. Between vortex-shedding events, the sphere and rings evolve according to (6). Each time a ring is shed, the momentum of the sphere changes discretely to preserve the linear impulse in the system overall.

Suppose there are N rings, with circulations Γ_i, present in $\mathcal{D}$ prior to a vortex-shedding event. We denote the linear impulse due to these N rings by P_N and the velocity of the fluid on the sphere across the shedding contour due to these N rings by $u_{v_t}(\theta)$. The velocity of the fluid on the sphere across the shedding contour due to the motion of the sphere is of the form $k_t\mathbf{U}$, where and k_t is obtained from (4). Let the tangential fluid velocity induced across the shedding contour by a newly shed vortex ring of *unit* circulation be $\Delta u_{v_t}(\theta)$ and let the linear impulse due to such a ring be ΔP. When introducing a new ring, we require that

$$\begin{pmatrix} \Delta u_{v_t}(\theta) & k_t - \sin\theta \\ \Delta P & M \end{pmatrix}\begin{pmatrix} \Gamma_{N+1} \\ \mathbf{U} \end{pmatrix} = \begin{pmatrix} -u_{v_t}(\theta) - a\dot{\theta} \\ L - P_N \end{pmatrix}. \tag{7}$$

On the right-hand side of (7) are velocities and momenta before the $(N+1)$th vortex ring is shed while Γ_{N+1} and $\mathbf{U}$ are the circulation of the $(N+1)$th ring and the velocity of the sphere at the instant of shedding. In (7), it's assumed

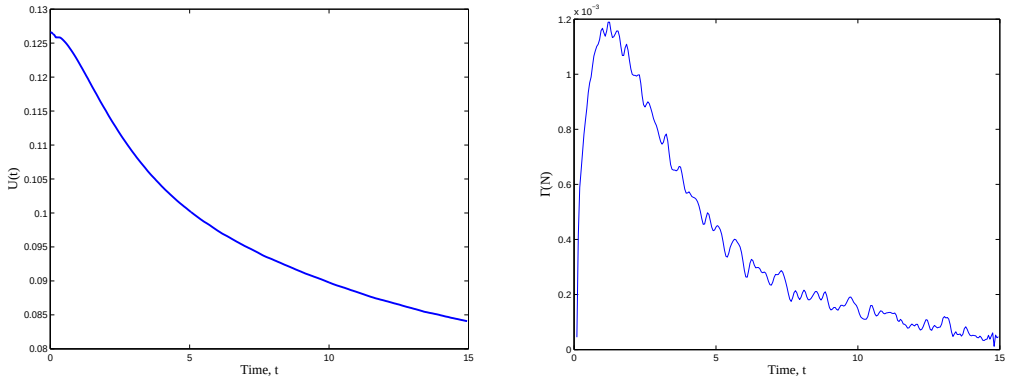

FIG. 4: Deceleration of a sphere with radius $a = 1$ shedding vortex rings adjacent to the contour $\theta = \pi/2$. The sphere's initial speed corresponds to unit linear impulse in the system in the absence of vortex rings; the total linear impulse is conserved as momentum is transferred from the sphere to the fluid. The sphere's speed in the positive z direction is shown as a function of time on the left and the strength of the most recently shed ring is shown as a function of time on the right.

while calculating $\Delta u_{v_t}(\theta)$ that the $(N+1)$th ring is shed at a distance d from the surface of the sphere with an initial radius of $(a+d)\sin\theta$.

III. SIMULATION

A. Drag due to vortex shedding

Before exploring our model's ability to mimic the propulsive mechanism depicted in Fig. 1, we consider the dynamics that result when the azimuthal angle θ specifying the position of the shedding contour on the sphere is fixed and the sphere is given an initial translational velocity along the z axis. In this case, vortex shedding constitutes a source of drag on the sphere.

For simplicity's sake, suppose that $\theta = \pi/2$, so that the shedding contour is maximally distant from the z axis. In this case, every shed ring will have the same sign, and the creation of each will diminish the sphere's velocity as momentum is transferred from the sphere to the fluid. Fig. 4 depicts a simulation of this phenomenon. As the sphere decelerates, the strengths of the rings it sheds decrease similarly.

B. Propulsion via periodic changes in ridge position

We now consider the effect of periodic variations in the azimuthal angle θ, corresponding conceptually to undulations in the shape of the swimmer in Fig. 1. We consider four distinct swimming gaits during which θ varies continuously between $\pi/2$ and $3\pi/4$. The shedding ridge moves at the same speed during the forward stroke in each case — in other words, as θ increases from $\pi/2$ to $3\pi/4$ — but recovers differently during each reverse stroke. In particular, we set

$$\dot{\theta}(t) = 12.5\pi^2 \sin 100\pi t \tag{8}$$

during the forward stroke in every case and choose

$$\begin{aligned} \text{case 1:} \quad & \dot{\theta}(t) = -(1/2)12.5\pi^2 \sin 100\pi t \\ \text{case 2:} \quad & \dot{\theta}(t) = -(1/3)12.5\pi^2 \sin 100\pi t \\ \text{case 3:} \quad & \dot{\theta}(t) = -(1/4)12.5\pi^2 \sin 100\pi t \\ \text{case 4:} \quad & \dot{\theta}(t) = -(1/5)12.5\pi^2 \sin 100\pi t \end{aligned} \tag{9}$$

for the four reverse strokes. If the proscription on flow across the shedding contour is enforced every 0.001 units of time, it follows that ten vortex rings are shed during each forward stroke.

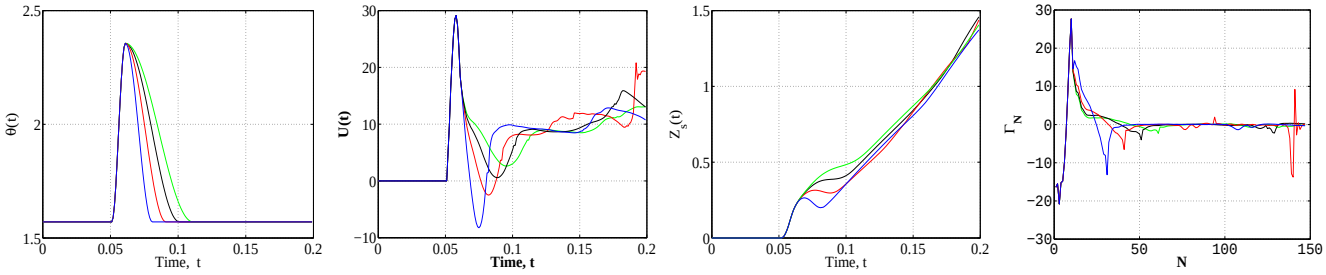

FIG. 5: Azimuthal position of the shedding contour (far left), sphere velocity (center left), sphere displacement (center right), and strength of the most recently shed ring (far right) resulting from the forward stroke (8) followed by each of the four reverse strokes (9). Case 1 is shown in blue, case 2 in red, case 3 in black, and case 4 in green.

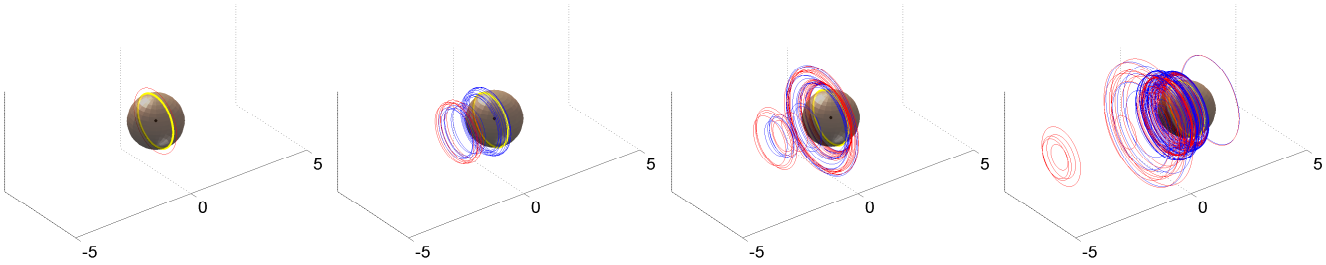

FIG. 6: Snapshots from the simulation corresponding to case 4 in Fig. 5. The shedding contour on the sphere is shown in yellow. Vortex rings with positive and negative circulation are shown in blue and red, respectively.

Fig. 5 depicts the resulting dynamics of the sphere and the shed vortex rings. In each case, the shedding ridge executes one forward stroke followed by one reverse stroke. We observe that the net displacement at $t = 0.15$ is nearly the same in all four cases. In the first two cases, the sphere briefly acquires a negative velocity during the reverse stroke, indicating that a slower reverse stroke is required to produce continuous forward motion. The absolute values of the circulations of the rings shed during the reverse stroke are smaller if the reverse stroke is slower. Fig. 6 shows the sphere and rings at different instants of time for case 4. An interesting observation in our simulations is the rapid leap-frogging of rings, a phenomenon that has been rigorously proved to exist in the case of three rings [25].

Additional swimming gaits can be defined by alternating periods of variation in θ with periods of relaxation during which θ is fixed. Figs. 7 and 8 depict a gait in which cyclic movements of the shedding ridge parametrized by (8) and (9) (case 1) alternate with periods of relaxation. The position of the ridge on the sphere oscillates four times, pausing for an interval of 0.01 units of time between the conclusion of each oscillation and the beginning of the next. The sphere accelerates from rest in the positive z direction, but will eventually approach a finite terminal average velocity. The strength of the most recently shed ring varies nearly periodically.

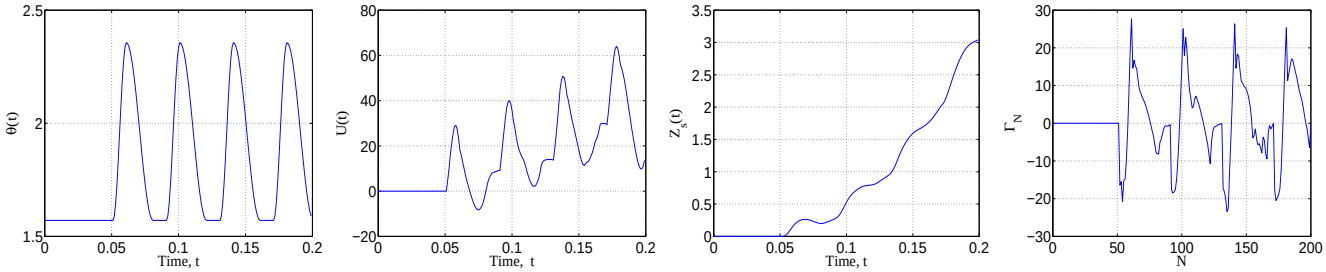

FIG. 7: Azimuthal position of the shedding contour (far left), sphere velocity (center left), sphere displacement (center right), and strength of the most recently shed ring (far right) resulting from a periodic gait alternating cyclic motions of the shedding ridge parametrized by (8) and (9) (case 1) with intervals of relaxation.

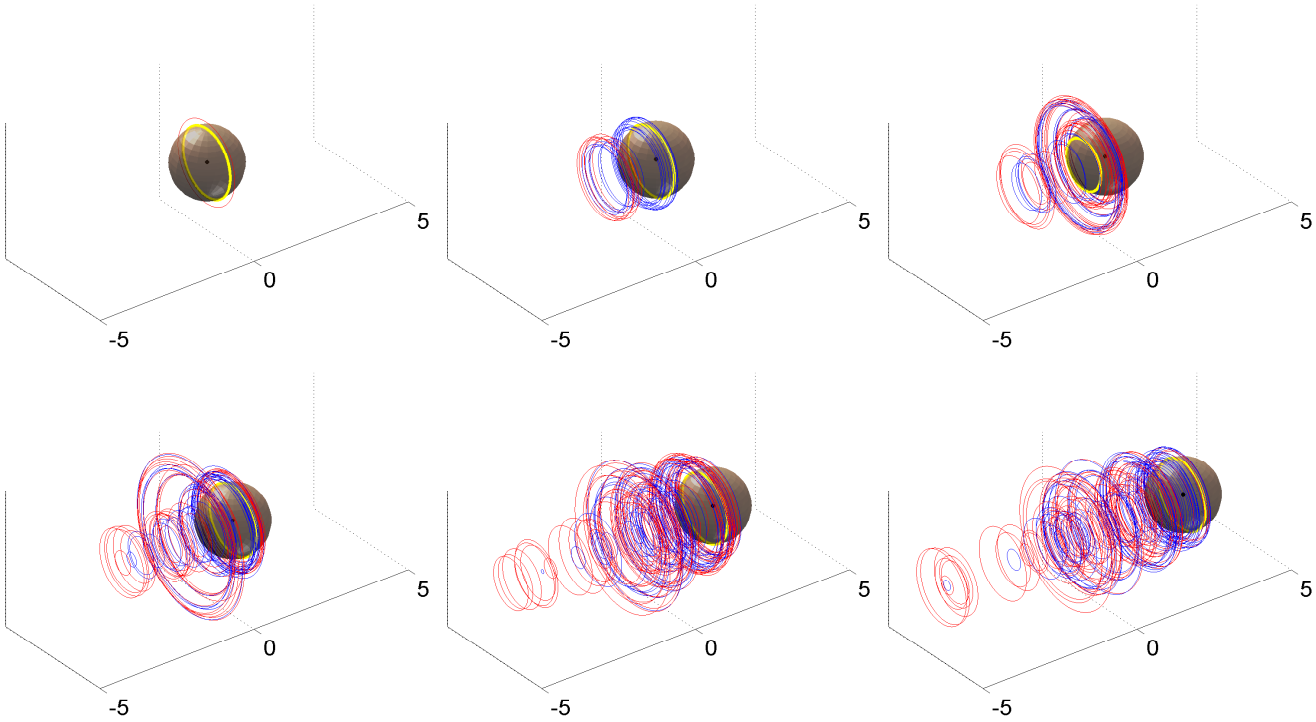

FIG. 8: Snapshots from the simulation corresponding to Fig. 7. The shedding contour on the sphere is shown in yellow. Vortex rings with positive and negative circulation are shown in blue and red, respectively.

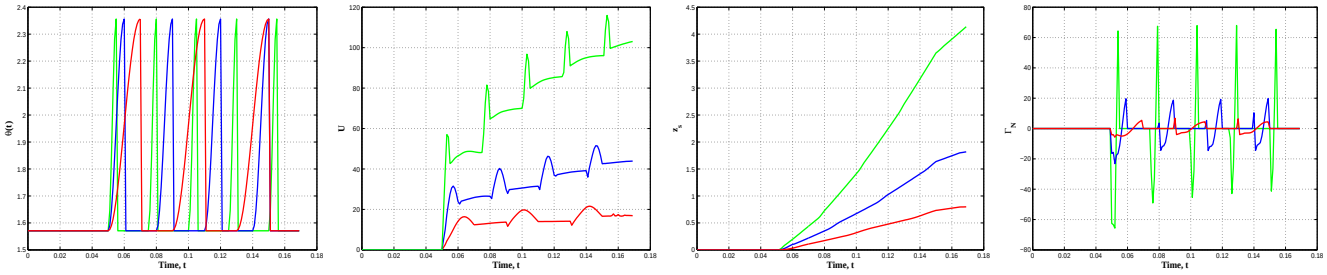

FIG. 9: Azimuthal position of the shedding contour (far left), sphere velocity (center left), sphere displacement (center right), and strength of the most recently shed ring (far right) resulting from three different periodic gaits in which vortex shedding occurs only during forward strokes. Intervals between forward strokes are depicted arbitrarily as rapid reverse strokes followed by periods of relaxation.

Figs. 5 and 7 both illustrate the decelerating effect a reverse stroke can have on the sphere. This phenomenon underscores the crudeness of the system we've described as a model for a swimmer like that depicted in Fig. 1, which would likely exploit more than one degree of freedom in its body shape to realize efficient propulsive gaits. In particular, a real swimmer would likely seek to temper the adverse influence of a reverse stroke by streamlining its body during recovery from a forward stroke. We can mimic this by suppressing the mechanism for vortex shedding in our model during reverse strokes, imagining the shedding ridge to be drawn periodically into the sphere as θ oscillates in value. Fig. 9 illustrates the effect of such an amendment to the model. Suppressing vortex shedding significantly mitigates the retarding influence of recovery from each forward stroke.

IV. DISCUSSION AND FUTURE WORK

A variety of models exist for the self-propulsion of deformable bodies in fluids, but the incorporation of vortex shedding as a mechanism for propulsion in such models has traditionally required a departure from analytical mechanics and the adoption of a purely computational perspective. The grounding of the model described herein — and of the model described in [8] — to the formalism of Hamiltonian mechanics offers the promise of rendering problems in biomorphic locomotion accessible to a variety of tools for analysis and for model-based control design. The Hamiltonian in the present context provides a means for assessing the energetics of propulsion through the shedding of circular vortex rings and for exploring the possibility of wake drafting and energy recapture among arrays of medusan swimmers. The authors intend both to extend the present model to accommodate body deformations and multi-directional swimming and to explore methods for reducing the present model dimension, particularly as the phase space grows with progressive vortex shedding.

V. ACKNOWLEDGMENTS

The authors thank B. N. Shashikanth and Tapobrata Bhattacharya for their helpful suggestions concerning the model described in Section II. The material presented herein is based on work supported by the National Science Foundation under grant CMMI-1000652.

[1] J. O. Dabiri, S. P. Colin, J. H. Costello, and M. Gharib. Flow patterns generated by oblate medusan jellyfish: Field measurements and laboratory analyses. *Journal of Experimental Biology*, 208:1257–1265, 2005.
[2] T. von Kármán. *Aerodynamics: Selected Topics in Light of Their Historical Development*. Dover, 2004.
[3] C. E. Brown and W. H. Michael. Effect of leading edge separation on the lift of a delta wing. *Journal of the Aeronautical Sciences*, 21(690–694 & 706), 1954.
[4] T. Sarpkaya and R. L. Schoaff. Inviscid model of two-dimensional vortex shedding by a circular cylinder. *AIAA Journal*, 17:1193–1200, 1979.
[5] G. S. Triantafyllou, M. S. Triantafyllou, and M. A. Grosenbaugh. Optimal thrust development in oscillating foils with application to fish propulsion. *Journal of Fluids and Structures*, 7:205–224, 1993.
[6] R. J. Mason and J. W. Burdick. Propulsion and control of deformable bodies in an ideal fluid. In *Proceedings of the IEEE International Conference on Robotics and Automation*, 1999.
[7] S. D. Kelly and H. Xiong. Self-propulsion of a free planar hydrofoil with localized vortex shedding: Analytical modeling and model reduction for control. In *Proceedings of the ASME Dynamic Systems and Control Conference*, 2008.
[8] S. D. Kelly and H. Xiong. Self-propulsion of a free hydrofoil with localized discrete vortex shedding: Analytical modeling and simulation. *Theoretical and Computational Fluid Dynamics*, 24(1):45–50, 2010.
[9] S. Michelin and S. G. Llewellyn Smith. An unsteady point vortex method for coupled fluid-solid problems. *Theoretical and Computational Fluid Dynamics*, 23:127–153, 2009.
[10] S. Michelin and S. G. Llewellyn Smith. Falling cards and flapping flags: Understanding fluid solid interactions using an unsteady point vortex model. *Theoretical and Computational Fluid Dynamics*, 24(1):195–200, 2010.
[11] P. Tallapragada and S. D. Kelly. Reduced-order modeling of propulsive vortex shedding from a free pitching hydrofoil with an internal rotor. To appear in *Proceedings of the 2013 American Control Conference*.
[12] S. M. Ramodanov. Motion of a circular cylinder and n point vortices in an ideal fluid. *Regular and Chaotic Dynamics*, 7(3):291–298, 2002.
[13] B. N. Shashikanth, J. E. Marsden, J. W. Burdick, and S. D. Kelly. The Hamiltonian structure of a 2-d rigid circular cylinder interacting dynamically with n point vortices. *Physics of Fluids*, 14:1214–1227, 2002.
[14] A. V. Borisov, I. S. Mamaev, and S. M. Ramodanov. Motion of a circular cylinder and n point vortices in an ideal fluid. *Regular and Chaotic Dynamics*, 8(4):449–462, 2003.
[15] B. N. Shashikanth. Poisson brackets for the dynamically interacting system of a 2d rigid cylinder and n point vortices: the case of arbitrary smooth cylinder shapes. *Regular and Chaotic Dynamics*, 10(1):1–14, 2005.
[16] B. N. Shashikanth, A. Sheshmani, S. D. Kelly, and J. E. Marsden. Hamiltonian structure for a neutrally buoyant rigid body interacting with n vortex rings of arbitrary shape: the case of arbitrary smooth body shape. *Theoretical and Computational Fluid Dynamics*, 22(1):37–64, 2008.
[17] B. N. Shashikanth, A. Sheshmani, S. D. Kelly, and M. Wei. Hamiltonian structure and dynamics of a neutrally buoyant rigid sphere interacting with thin vortex rings. *Journal of Mathematical Fluid Mechanics*, 2010. DOI 10.1007/s00021-008-0291-0.
[18] Sir H. Lamb. *Hydrodynamics*. Dover, 1945.
[19] P. G. Saffman. *Vortex Dynamics*. Cambridge University Press, 1992.
[20] P. Weiss. On hydrodynamical images: Arbitrary irrotational flow disturbed by a sphere. *Proceedings of the Cambridge Philosophical Society*, 40:259–261, 1944.

[21] O. M. Knio and L. Ting. Vortical flow outside a sphere and sound generation. *SIAM Journal of Applied Mathematics*, 57:972–981, 1997.
[22] P. K. Newton. *The N-Vortex Problem*. Springer-Verlag, 2001.
[23] B. N. Shashikanth and J. E. Marsden. Leap-frogging vortex rings: Hamiltonian structure, geometric phases and discrete reduction. *Fluid Dynamics Research*, 33(4):333–356, 2003.
[24] L. M. Milne-Thomson. *Theoretical Hydrodynamics*. Dover, 1996.
[25] A. V. Borisov, A. A. Kilin, and I. S. Mamaev. The dynamics of vortex rings: Leapfrogging, choreographies and the stability problem. *Russian Journal of Nonlinear Dynamics*, 8(1):113–147, 2012.